Electronic Supplementary Material (ESI) for Journal of Materials Chemistry C.

Supporting Information

"Hot-Nodes" Controlled Facile Synthesis of 3D Rare Earth Micro-Networks with Symmetry Deviation Induced High Luminescence

Bin-Bin Chen, Jian Lv, Shuai Chang, Xiao-Yuan Wang, Ruo-Can Qian* and Da-Wei Li

East China University of Science and Technology

*E-mail: ruocanqian@ecust.edu.cn

Supplementary Note 1. Illustration of the synthesis process of RE-MNs.

High luminescent RE-MNs were prepared through one-pot hydrothermal synthesis. The production yields of Eu-MNs and Tb-MNs were 3.7% and 28.0%, respectively.

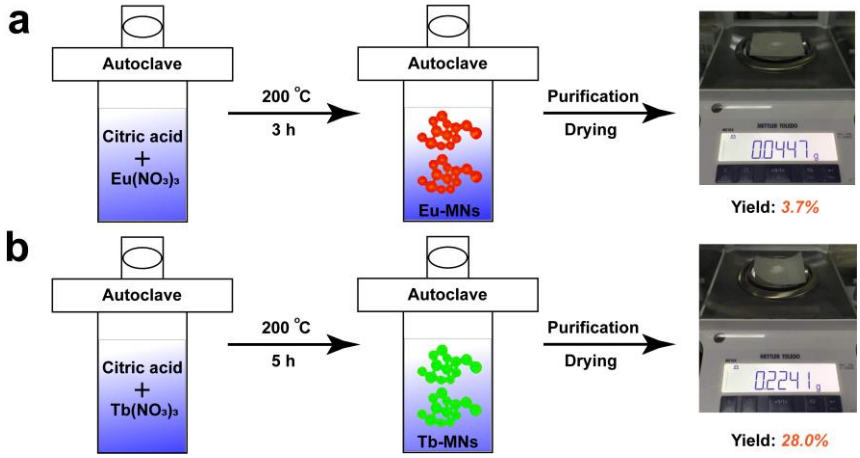

Figure S1. Illustration of the synthesis process of (a) Eu-MNs and (b) Tb-MNs.

Supplementary Note 2. Thermogravimetric analysis of RE-MNs

The thermal stability of RE-MNs in nitrogen environment was measured through a thermogravimetric (TGA) 8000 thermogravimetry. The temperature range was from 35 to 800 ^{o}C and the heating rate was 10 ^{o}C/min. The slow weight loss appearing in the temperature below 300 ^{o}C corresponds to the loss of physisorbed and coordinated water. The rapid weight loss appearing in the temperature range above 300 ^{o}C may be due to decomposition of RE-MNs. The final residuals of Eu-MNs and Tb-MNs were 50.20% and 62.24%, respectively.

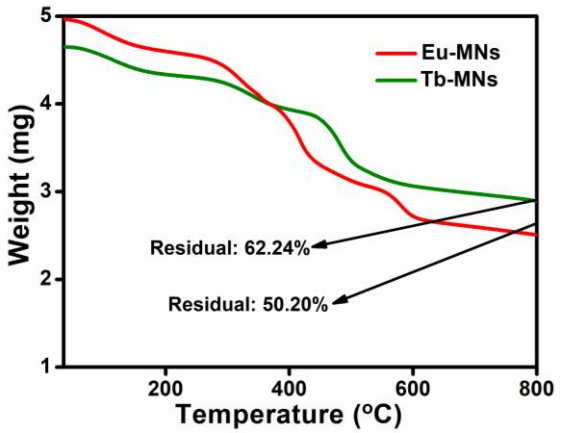

Figure S2. Thermogravimetric curves of RE-MNs.

Supplementary Note 3. FT-IR spectra of Tb^{3+}/CA complex and Tb-MNs.

The FT-IR spectra of Tb^{3+}/CA complex and Tb-MNs were measured through a Fourier Transform Infrared spectrometer. The FT-IR spectrum (Figure S3a) of Tb^{3+}/CA complex was similar with the Eu^{3+}/CA complex. Two strong bands centered at about 1383 and 1615 cm^{-1} correspond to the symmetrical and asymmetrical vibrations of the carboxylate groups of citrate, respectively[1], which indicated that the carboxyl groups coordinate to the Tb^{3+} ions. Two peaks at about 1079 and 1211 cm^{-1} characterized the C-O stretching vibrations of the citrate.[2] The broad absorption band located at ~ 3411 cm^{-1} characterized the hydroxyl groups of Tb^{3+}/CA complex at weak surface active sites with which physisorbed water molecules were bound by weak hydrogen bonds, while the absorption at ~ 3188 cm^{-1} was associated with coordinated water molecules that were strongly bound to the Tb^{3+} ions in Tb^{3+}/CA complex through Tb-O bond.[3, 4] Meanwhile, the FT-IR spectrum (Figure S3b) of Tb-MNs was also similar with the Eu-MNs. After the formation of Tb-MNs, and the $\Delta\nu$ ($\nu_{s(COO^-)}$ - $\nu_{as(COO^-)}$) was also reduced, indicating that one CA ligand combined more Tb^{3+} ions. Moreover, the stretching vibration of C=O at about 1725 cm^{-1} disappeared completely after the formation of Tb-MNs also confirmed the mass formation of carboxylates. The similar change trends in FT-IR spectra indicated the formation processes of Tb-MNs were consistent with the Eu-MNs.

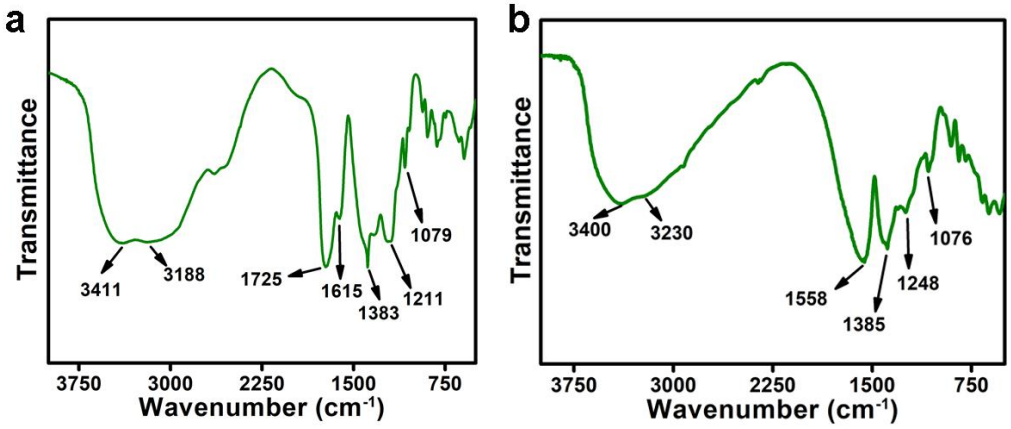

Figure S3. FT-IR spectra of (a) Tb^{3+}/CA complex and (b) Tb-MNs.

Supplementary Note 4. SEM image of 2D microsheet.

The SEM image of 2D microsheet was obtained through a field emission scan electron microscopy. The intermediate product during the synthesis of Eu-MNs, that was 2D microsheet, could be obtained by ending the reaction 1.5 h in advance.

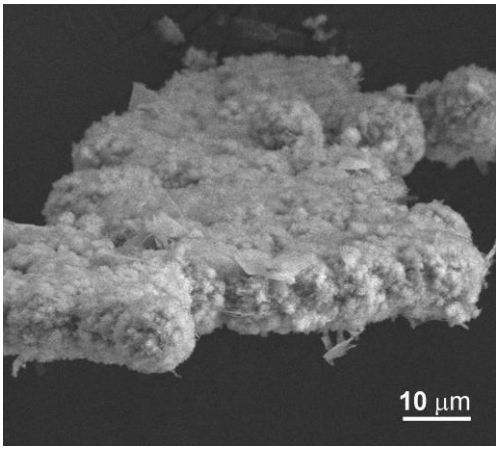

Figure S4. SEM image of 2D microsheet. Reaction time: 1.5 h.

Supplementary Note 5. SEM images of the hot-nodes.

The SEM images of the hot-nodes were obtained through a field emission scan electron microscopy. The appearance and final formation of hot-nodes usually taken place when the reaction time was 2 h. Figure S5a and b clearly showed that hot-nodes begin to appear on the 2D microsheet and the hot-nodes varied in size and consisted of many small flakes. As the reaction continued, the hot-nodes in 2D microsheet gradually became larger and relatively uniform through Oswald ripening process (Figure S5c and d).

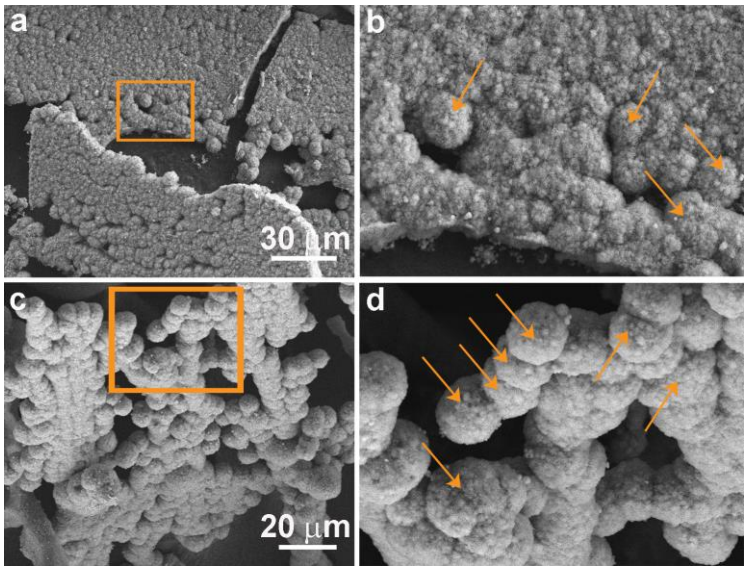

Figure S5. SEM images of the hot-nodes. (a) SEM image of hot-nodes at the beginning. (b) The enlarged SEM image corresponding to the square box area in (a). Arrows referred to hot-nodes of different sizes. (c) SEM image of fully formed larger hot-nodes. (d) The enlarged SEM image corresponding to the square box area in (c). Arrows referred to hot-nodes. Reaction time: 2 h.

Supplementary Note 6. XRD spectra of RE-MNs.

The XRD spectra of RE-MNs were measured through a rotating anode X-ray powder diffractometer. The XRD spectra of RE-MNs showed a broad diffraction peak centered at about 44.5º, indicating that RE-MNs had a non-crystalline structure.

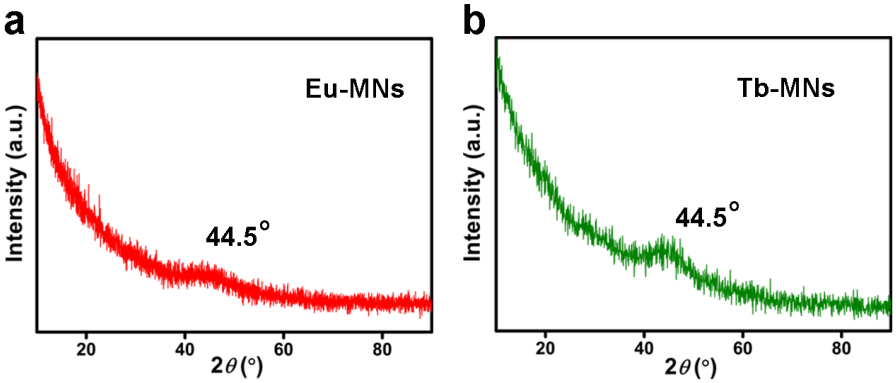

Figure S6. XRD spectra of (a) Eu-MNs and (b) Tb-MNs.

Supplementary Note 7. The large-area surface morphology of Eu-MNs.

The large-area surface morphology image of Eu-MNs was obtained through a common fluorescence microscope. The size of Eu-MNs could reach 1.30 mm at length × 0.75 mm at width. Therefore, a high-quality and large-area 3D RE-MNs could be easily synthesized by hot-node controlled synthesis technology.

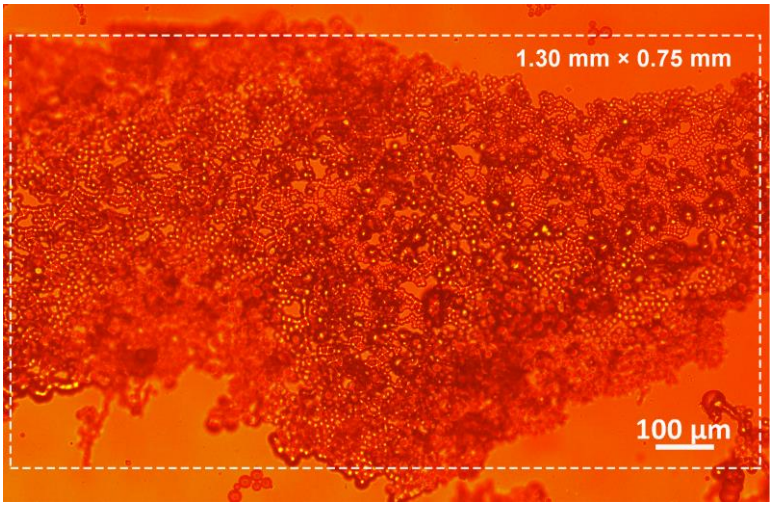

Figure S7. The large-area surface morphology of Eu-MNs.

Supplementary Note 8. Element mapping at the section of single hot-node in RE-MNs.

The element mapping at the section of single hot-node in RE-MNs were obtained through an EDS used in combination with a field emission scan electron microscopy. Similar to the results of surface element mapping, two RE-MNs were consisted of carbon, oxygen and RE elements. The shadow part (dashed box) in Eu-MNs and Tb-MNs was caused by the unevenness (solid box) of the cut plane, rather than nonuniform ingredients.

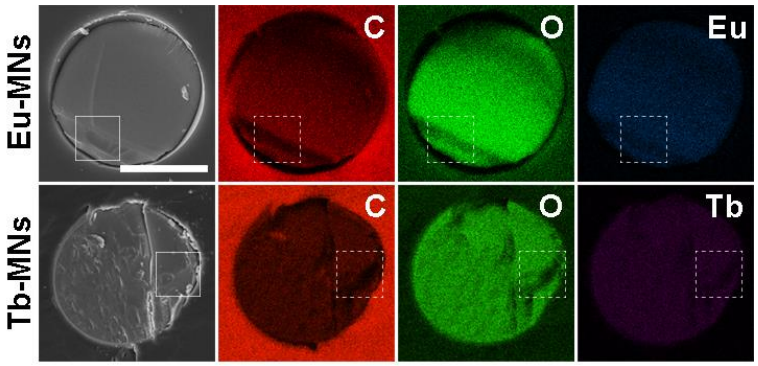

Figure S8. Element mapping at the section of single hot-node in RE-MNs. Scale bar, 10 μm.

Supplementary Note 9. XPS spectra of RE-MNs.

The elemental composition of RE-MNs was measured through an X-ray photoelectron spectrometer. Results showed that RE-MNs were consisted of RE, carbon and oxygen elements. The XPS spectrum analysis of Eu-MNs showed that C1s, O1s, Eu3d and Eu4d peaks were located about at 284.8, 531.64, 1134.82 eV and 135.18 eV (Fig. S9a), respectively.[5] The XPS spectrum analysis of Tb-MNs showed that C1s, O1s, Tb3d and Tb4d peaks were located about at 288.48, 531.52, 1242.75 eV and 151.01 eV (Fig. S9d), respectively.[6] The high-resolution C1s and O1s spectra of two RE-MNs were very similar, indicating that the structures of two RE-MNs were consistent.

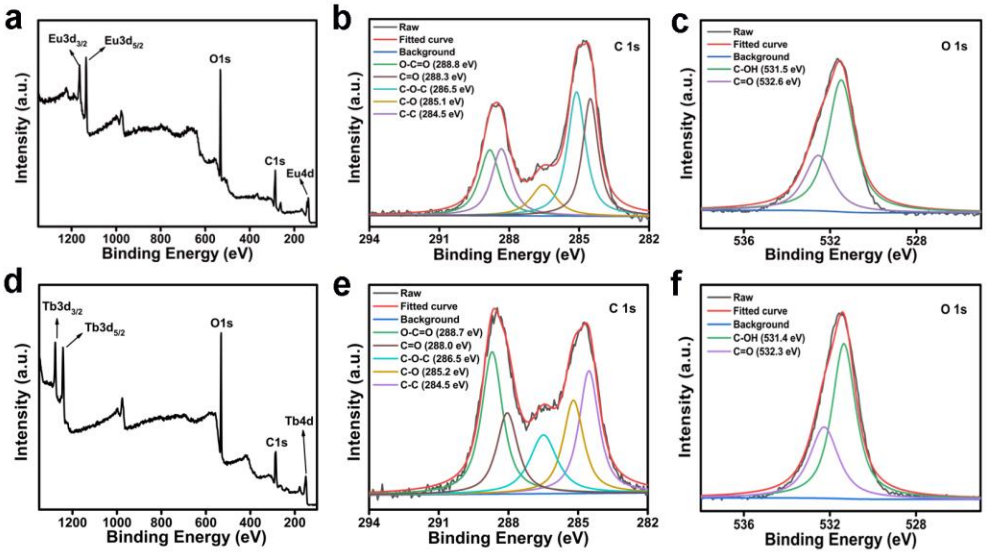

Figure S9. XPS spectra of RE-MNs. The (a) full XPS, (b) C1s, and (c) O1s spectra of Eu-MNs. The (d) full XPS, (e) C1s, and (f) O1s spectra of Tb-MNs.

Supplementary Note 10. The 2D and 3D PL images of RE-MNs in aqueous solution.

The 2D and 3D PL images of RE-MNs were obtained through laser confocal microscope. The 3D PL imaging showed that RE-MNs were spatially well-defined and highly-ordered.

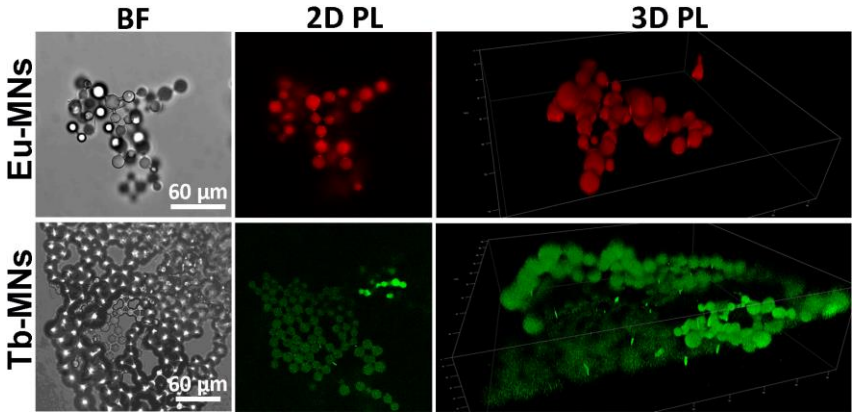

Figure S10. The 2D and 3D PL images of RE-MNs in aqueous solution. Excitation wavelength: 405 nm.

Supplementary Note 11. Absorption spectrum of CA.

The absorption spectrum of CA in aqueous solution was measured through a USB 2000+ spectrometer. The concentration of CA was 0.02 M. Result showed that electronic absorption spectrum of CA was located in a shortwave UV region of 200–250 nm. Because CA had only an n-π* transition of C=O, the CA had the characteristics of small extinction coefficient (ε < 100). Therefore, the CA showed very weak light absorption.

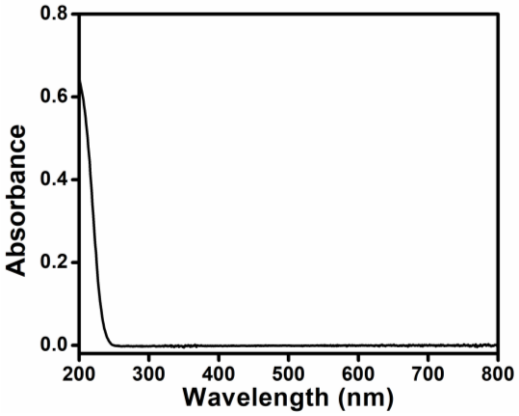

Figure S11. Absorption spectrum of CA.

Supplementary Note 12. Phosphorescence spectrum of Gd^{3+}/CA complex.

Phosphorescence spectrum of Gd^{3+}/CA complex was determined at 77 K. The Gd complex was chosen as the model compound to determine the triplet state energy levels of organic ligand because of its high phosphorescence/fluorescence ratio compared with other RE complexes. The reciprocal of the shortest emission wavelength in the phosphorescence spectrum was the lowest triplet state energy level (T1) of the ligand. As shown in Figure S12, the shortest emission wavelength of Gd^{3+}/CA complex was at 434 nm, so the lowest triplet state energy level of CA was 23042 cm^{-1}. This value was similar to the theoretical value (23582 cm^{-1}) obtained by Gaussian09.

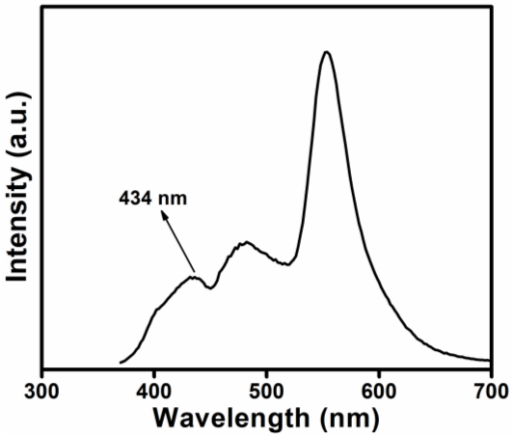

Figure S12. Phosphorescence spectrum of Gd^{3+}/CA complex. Excitation wavelength: 350 nm.

Supplementary Note 13. Schematic diagram of ET between RE^{3+} ions and CA ligand.

It is generally believed that the luminescent mechanism of RE complex as follow:[7] the CA ligand absorbs the external light energy, the transition of electrons from the ground state (S_0) to the excited singlet (S_1), and then to the lowest triplet (T_1) of the CA ligand through the intersystem crossing (ISC). Then, the lowest excited triplet transfers the energy to the RE^{3+} ions through a non-radiative energy transfer (ET). The characteristic PL of RE^{3+} ions was produced by the transition from the different vibration energy level of RE^{3+} ions to the ground state. The lowest excited state energy level of Eu^{3+} ions ($^5D_0$) and Tb^{3+} ions ($^5D_4$) were 17250 cm^{-1} and 20430 cm^{-1}, respectively. In our experiment, CA ligand could transfer absorbed energy to Eu^{3+} ions and Tb^{3+} ions. However, due to weak light absorption ability of CA and the mismatched energy level of CA and RE^{3+} ions, the RE^{3+}/CA complexes were low-luminescent.

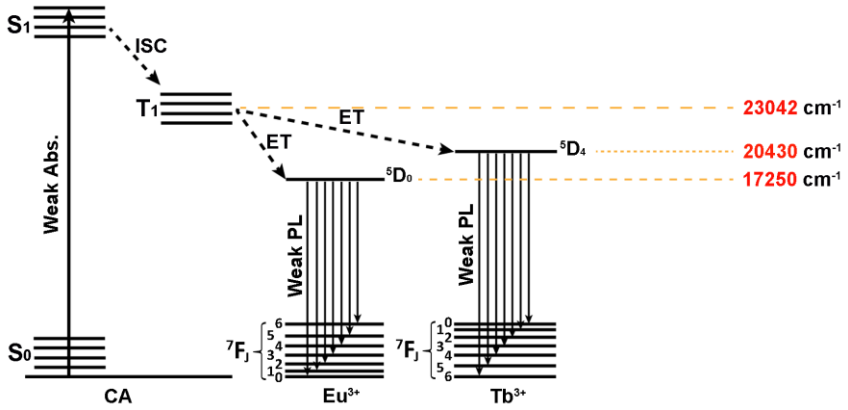

Figure S13. Schematic diagram of ET between RE^{3+} ions and CA ligand.

Supplementary Note 14. Excitation and emission spectra of RE^{3+}/CA complexes.

The excitation and emission spectra of RE^{3+}/CA complexes was measured through a fluorescence spectrophotometer. The emission spectrum (Figure S14c) of Eu^{3+}/CA complex showed characteristic emission peaks at 578 nm, 591 nm, 616 nm, 650 nm and 697 nm, respectively, corresponding to $^5D_0 \rightarrow {}^7F_0$, $^5D_0 \rightarrow {}^7F_1$, $^5D_0 \rightarrow {}^7F_2$, $^5D_0 \rightarrow {}^7F_3$, and $^5D_0 \rightarrow {}^7F_4$ transitions. The emission spectrum (Figure S14d) of Tb^{3+}/CA complex showed characteristic emission peaks at 488 nm, 545 nm, 583 nm, and 620 nm, respectively, corresponding to $^5D_4 \rightarrow {}^7F_6$, $^5D_4 \rightarrow {}^7F_5$, $^5D_4 \rightarrow {}^7F_4$, and $^5D_4 \rightarrow {}^7F_3$ transitions.

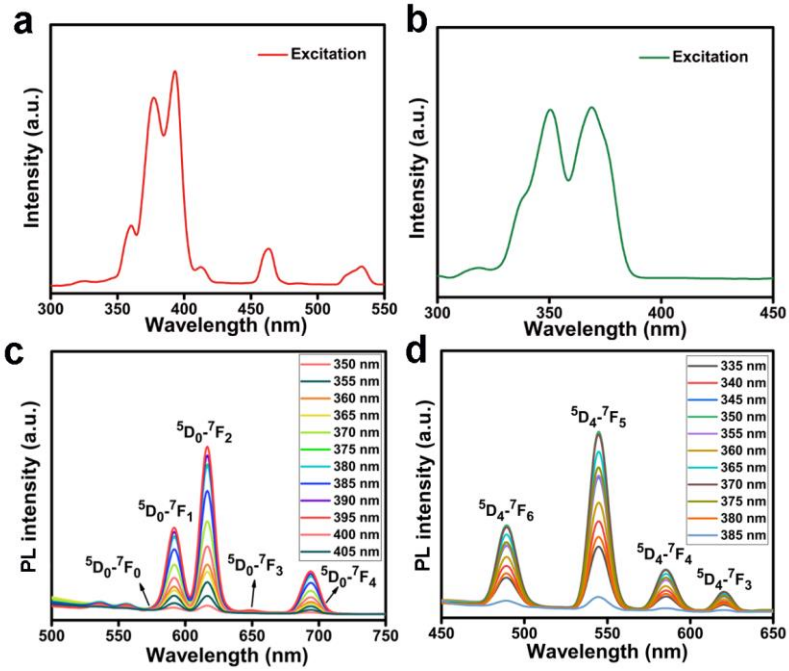

Figure S14. Excitation and emission spectra of RE^{3+}/CA complexes. (a) The excitation spectrum of Eu^{3+}/CA complex. Em = 616 nm. (b) The excitation spectrum of Tb^{3+}/CA complex. Em = 545 nm. The emission spectra of (c) Eu^{3+}/CA complex and (d) Tb^{3+}/CA complex under differnt excitation wavelengths.

Supplementary Note 15. Absorption spectra of RE^{3+}/CA complexes.

The absorption spectra of RE^{3+}/CA complex in aqueous solution were measured through a USB 2000+ spectrometer. The absorption spectra of RE^{3+}/CA complexes had no line-type absorption bands, indicated that the f-f transition was almost forbidden in RE^{3+}/CA complexes.

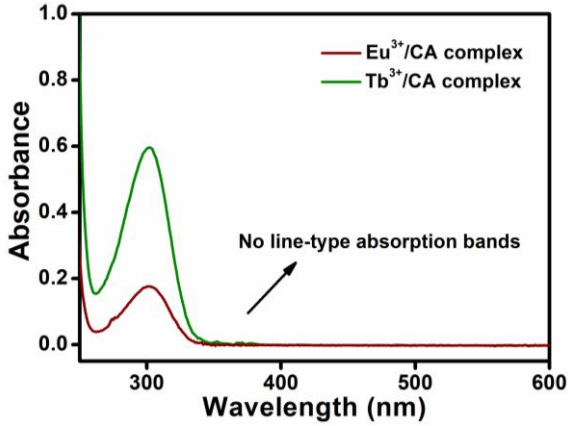

Figure S15. Absorption spectra of RE^{3+}/CA complexes.

Supplementary Note 16. The intensity ratio between $^5D_0 - {}^7F_2$ and $^5D_0 - {}^7F_1$ transitions of Eu^{3+}/CA complex and Eu-MNs.

The $^5D_0 - {}^7F_2$ transition is an electric-dipole transition. The intensity of $^5D_0 - {}^7F_2$ transition directly depends on the symmetry of Eu^{3+} ion in the environment. When Eu^{3+} ion is strictly in the center of inversion, this $^5D_0 - {}^7F_2$ transition cannot be observed. However, as the symmetry of Eu^{3+} ion decreases, the $^5D_0 - {}^7F_2$ transition will become stronger. While the $^5D_0 - {}^7F_1$ transition is a magnetic-dipole transition. The emission intensity caused by the $^5D_0 - {}^7F_1$ transition is not affected by the coordination environment of Eu^{3+} ion. Therefore, the intensity ratio between $^5D_0 - {}^7F_2$ and $^5D_0 - {}^7F_1$ transitions can be used to distinguish the symmetry change of Eu^{3+} ion in coordination environment.[8]

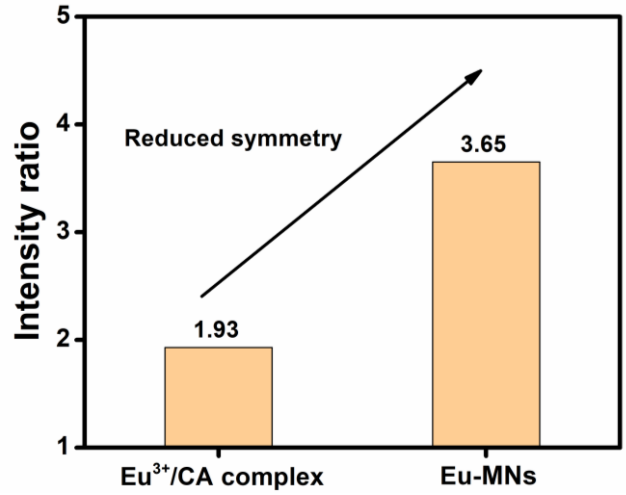

Figure S16. The intensity ratio between $^5D_0 - {}^7F_2$ and $^5D_0 - {}^7F_1$ transitions of Eu^{3+}/CA complex and Eu-MNs.

Supplementary Note 17. PL decay curves of RE^{3+}/CA complexes.

The PL lifetimes of RE^{3+}/CA complexes were measured through a FLS980 fluorescence spectrometer. As shown in Figure S17a, the PL decay curve of Eu^{3+}/CA complex was fitted by double exponential method (ExpDec2), and the equation:

$$y = 2036.1 * \exp(-x/148058.7) + 3254.8 * \exp(-x/148062.6) - 6.9$$

As shown in Figure S17b, the PL decay curve of Tb^{3+}/CA complex was fitted by double exponential method (ExpDec2), and the equation:

$$y = 1626.5 * \exp(-x/712.1) + 3292.2 * \exp(-x/496536.2) - 0.9$$

According to the following equation:

$$\tau_{avg} = (A_1 * \tau_1^2 + A_2 * \tau_2^2)/(A_1 * \tau_1 + A_2 * \tau_2)$$

Therefore, the average PL lifetimes of Eu^{3+}/CA complex and Tb^{3+}/CA complex were 142797.6 ns and 497165.2 ns, respectively.

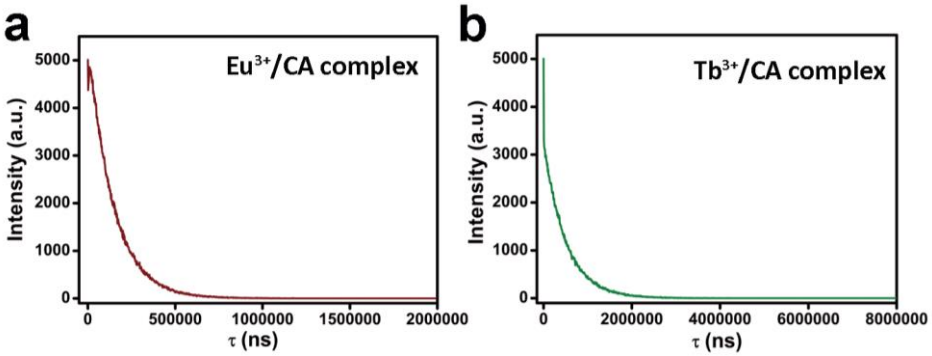

Figure S17. PL decay curves of (a) Eu^{3+}/CA complex and (b) Tb^{3+}/CA complex.

Table S1. The radiative and non-radiative rate constants of the RE^{3+}/CA complexes and RE-MNs.

	ϕ (%)	τ (ns)	k_r (s^{-1})	k_{nr} (s^{-1})
Eu^{3+}/CA complex	0.27	142797.6	18.9	7.0×10^4
Eu-MNs	36.25	2.36	1.5×10^8	2.7×10^8
Tb^{3+}/CA complex	0.36	497165.2	7.2	2.0×10^4
Tb-MNs	34.47	2.28	1.5×10^8	2.9×10^8

Table S2. Important photoelectric parameters for R-LEDs and G-LEDs with different correlated colour temperatures (CCTs).

Devices	Phosphor	CCT (K)	Chromaticity coordinate		Current (mA)	Efficacy (lm W^{-1})
			x	y		
R-LEDs	Eu-MNs	1004	0.6076	0.3061	20	1.18
		1023	0.6181	0.309	40	1.15
		1013	0.6154	0.3089	60	1.09
		1016	0.6226	0.3146	80	1.03
		1080	0.5854	0.3033	100	0.98
		1189	0.561	0.3041	120	0.92
G-LEDs	Tb-MNs	5604	0.3277	0.5756	20	3.77
		5719	0.3226	0.576	40	3.88
		5657	0.3253	0.5667	60	3.94
		5665	0.3253	0.5804	80	3.87
		5717	0.323	0.5642	100	3.77
		5671	0.3248	0.5442	120	3.69

Table S3. The comparison of optical properties of common red phosphors.

Red phosphor	λ_{max}	FWHM	Ref.
$CaAlSiN_3:Eu^{2+}$	644 nm / 647 nm	~ 125 nm	[9]
$Li_2Ca_2[Mg_2Si_2N_6]:Eu^{2+}$	638 nm	~ 86 nm	[10]
$Sr[Mg_3SiN_4]:Eu^{2+}$	~ 615 nm	~ 43 nm	[11]
$Ba[Mg_3SiN_4]:Eu^{2+}$	~ 670 nm	~ 88 nm	[12]
$Sr_4[LiAl_{11}N_{14}]:Eu^{2+}$	~ 670 nm	~ 85 nm	[13]
$Ca_{18.75}Li_{10.5}[Al_{39}N_{55}]:Eu^{2+}$	~ 647 nm	~ 53 nm	[14]
Eu-MNs	614 nm	~ 20 nm	This work

References

1. W. Tong, L. Li, W. Hu, T. Yan and G. Li, *J. Phys. Chem. C*, 2010, **114**, 1512-1519.
2. Y. Su, G. Li, Y. Xue and L. Li, *J. Phys. Chem. C*, 2007, **111**, 6684-6689.
3. T. Bezrodna, G. Puchkovska, V. Shimanovska, I. Chashechnikova, T. Khalyavka and J. Baran, *Appl. Surf. Sci.*, 2003, **214**, 222-231.
4. G. Li, L. Li, J. Boerio-Goates and B. F. Woodfield, *J. Am. Chem. Soc.*, 2005, **127**, 8659-8666.
5. L. P. Lin, X. H. Song, Y. Y. Chen, M. C. Rong, Y. R. Wang, L. Zhao, T. T. Zhao and X. Chen, *Anal. Chim. Acta*, 2015, **891**, 261-268.
6. B. B. Chen, Z. X. Liu, H. Y. Zou and C. Z. Huang, *Analyst*, 2016, **141**, 2676-2681.
7. N. Sabbatini, M. Guardigli and J.-M. Lehn, *Coordin. Chem. Rev.*, 1993, **123**, 201-228.
8. B. R. Judd, *J. Chem. Phys.*, 1966, **44**, 839-840.
9. H. S. Kim, K. Machida, T. Horikawa and H. Hanzawa, *J. Alloy. Comp.*, 2015, **633**, 97-103.
10. P. Strobel, V. Weiler, C. Hecht, P. J. Schmidt and W. Schnick, *Chem. Mater.*, 2017, **29**, 1377-1383.
11. S. Schmiechen, H. Schneider, P. Wagatha, C. Hecht, P. J. Schmidt and W. Schnick, *Chem. Mater.*, 2014, **26**, 2712.
12. S. Schmiechen, P. Strobel, C. Hecht, T. Reith, M. Siegert, P. Schmidt, P. Huppertz, D. Wiechert and W. Schnick, *Chem. Mater.*, 2015, **46**, 150205203715000.
13. D. Wilhelm, D. Baumann, M. Seibald, K. Wurst, G. Heymann and H. Huppertz, *Chem. Mater.*, 2016, **29**, 1204–1209.
14. P. Wagatha, P. Pust, V. Weiler, A. S. Wochnik, P. J. Schmidt, C. Scheu and W. Schnick, *Chem. Mater.*, 2016, **28**, 1220-1226.